First Measurement of Ξ^- Polarization in Photoproduction

J. Bono[a,b,1], L. Guo[a], B.A. Raue[a], S. Adhikari[a], M.C. Kunkel[c], K.P. Adhikari[af,2], Z. Akbar[p], M.J. Amaryan[af], J. Ball[j], L. Barion[t], M. Bashkanov[am], M. Battaglieri[u], V. Batourine[ak], I. Bedlinskiy[y], A.S. Biselli[n], W.K. Brooks[al], V.D. Burkert[ak], F. Cao[l], D.S. Carman[ak], A. Celentano[u], G. Charles[af], T. Chetry[ae], G. Ciullo[t,o], Brandon A. Clary[l], P.L. Cole[s], M. Contalbrigo[t], V. Crede[p], A. D'Angelo[v,ag], N. Dashyan[ar], R. De Vita[u], M. Defurne[j], A. Deur[ak], S. Diehl[l], C. Djalali[ai], M. Dugger[e], H. Egiyan[ak,ac], A. El Alaoui[al], L. El Fassi[ab], P. Eugenio[p], G. Fedotov[ae,ah], A. Filippi[w], A. Fradi[x,3], G. Gavalian[ak,af], N. Gevorgyan[ar], Y. Ghandilyan[ar], F.X. Girod[ak,j], D.I. Glazier[an], W. Gohn[l,4], E. Golovatch[ah], R.W. Gothe[ai], K.A. Griffioen[aq], K. Hafidi[d], N. Harrison[ak], M. Hattawy[d], D. Heddle[k,ak], K. Hicks[ae], M. Holtrop[ac], Y. Ilieva[ai], D.G. Ireland[an], E.L. Isupov[ah], H.S. Jo[aa], S. Johnston[d], M.L. Kabir[ab], D. Keller[ao,ae], G. Khachatryan[ar], M. Khachatryan[af], M. Khandaker[ad,5], A. Kim[l], W. Kim[aa], A. Klein[af], F.J. Klein[i], V. Kubarovsky[ak], P. Lenisa[t], K. Livingston[an], I .J .D. MacGregor[an], M. Markov[l], B. McKinnon[an], T. Mineeva[al,l], R.A. Montgomery[an], C. Munoz Camacho[x], G. Niculescu[z], M. Osipenko[u], A.I. Ostrovidov[p], M. Paolone[aj], R. Paremuzyan[ac], K. Park[ak,ai], E. Pasyuk[ak,e], W. Phelps[a], O. Pogorelko[y], J.W. Price[f], Y. Prok[ap,af], D. Protopopescu[an], M. Ripani[u], A. Rizzo[v,ag], G. Rosner[an], F. Sabatié[j], C. Salgado[ad], R.A. Schumacher[h], Y. Sharabian[ak], Iu. Skorodumina[ai,ah], G.D. Smith[am], D. Sokhan[an,am], N. Sparveris[aj], S. Stepanyan[ak], I.I. Strakovsky[r], S. Strauch[ai], M. Taiuti[q,6], J.A. Tan[aa], M. Ungaro[ak,l], H. Voskanyan[ar], E. Voutier[x], R. Wang[x], X. Wei[ak], M.H. Wood[g,ai], N. Zachariou[am], L. Zana[am,ac], J. Zhang[ao,af], Z.W. Zhao[af,ai,m]

[a] *Florida International University, Miami, Florida 33199*
[b] *Rice University, Houston, Texas 77005*
[c] *Institute fur Kernphysik (Juelich), Juelich, Germany*
[d] *Argonne National Laboratory, Argonne, Illinois 60439*
[e] *Arizona State University, Tempe, Arizona 85287-1504*
[f] *California State University, Dominguez Hills, Carson, CA 90747*
[g] *Canisius College, Buffalo, NY*
[h] *Carnegie Mellon University, Pittsburgh, Pennsylvania 15213*
[i] *Catholic University of America, Washington, D.C. 20064*
[j] *IRFU, CEA, Universit'e Paris-Saclay, F-91191 Gif-sur-Yvette, France*
[k] *Christopher Newport University, Newport News, Virginia 23606*
[l] *University of Connecticut, Storrs, Connecticut 06269*
[m] *Duke University, Durham, North Carolina 27708-0305*
[n] *Fairfield University, Fairfield CT 06824*
[o] *Universita' di Ferrara , 44121 Ferrara, Italy*
[p] *Florida State University, Tallahassee, Florida 32306*
[q] *Università di Genova, 16146 Genova, Italy*
[r] *The George Washington University, Washington, DC 20052*
[s] *Idaho State University, Pocatello, Idaho 83209*
[t] *INFN, Sezione di Ferrara, 44100 Ferrara, Italy*
[u] *INFN, Sezione di Genova, 16146 Genova, Italy*
[v] *INFN, Sezione di Roma Tor Vergata, 00133 Rome, Italy*
[w] *INFN, Sezione di Torino, 10125 Torino, Italy*
[x] *Institut de Physique Nucléaire, CNRS/IN2P3 and Université Paris Sud, Orsay, France*
[y] *Institute of Theoretical and Experimental Physics, Moscow, 117259, Russia*
[z] *James Madison University, Harrisonburg, Virginia 22807*
[aa] *Kyungpook National University, Daegu 41566, Republic of Korea*
[ab] *Mississippi State University, Mississippi State, MS 39762-5167*
[ac] *University of New Hampshire, Durham, New Hampshire 03824-3568*
[ad] *Norfolk State University, Norfolk, Virginia 23504*

Email addresses: jbono@fnal.gov (J. Bono), leguo@fiu.edu (L. Guo)

[1] Current address: Particle Physics Division, Fermi National Accelerator Laboratory, Batavia, IL 60510
[2] Current address: Mississippi State University, MS 39762-5167
[3] Current address: Imam Abdulrahman Bin Faisal University, Industrial Jubail 31961, Saudi Arabia
[4] Current address: LEXINGTON, KENTUCKY 40506
[5] Current address: Pocatello, Idaho 83209
[6] Current address: 16146 Genova, Italy

ae Ohio University, Athens, Ohio 45701
af Old Dominion University, Norfolk, Virginia 23529
ag Universita' di Roma Tor Vergata, 00133 Rome Italy
ah Skobeltsyn Institute of Nuclear Physics, Lomonosov Moscow State University, 119234 Moscow, Russia
ai University of South Carolina, Columbia, South Carolina 29208
aj Temple University, Philadelphia, PA 19122
ak Thomas Jefferson National Accelerator Facility, Newport News, Virginia 23606
al Universidad Técnica Federico Santa María, Casilla 110-V Valparaíso, Chile
am Edinburgh University, Edinburgh EH9 3JZ, United Kingdom
an University of Glasgow, Glasgow G12 8QQ, United Kingdom
ao University of Virginia, Charlottesville, Virginia 22901
ap Virginia Commonwealth University, Richmond, VA 23220
aq College of William and Mary, Williamsburg, Virginia 23187-8795
ar Yerevan Physics Institute, 375036 Yerevan, Armenia

Abstract

Despite decades of studies of the photoproduction of hyperons, both their production mechanisms and their spectra of excited states are still largely unknown. While the parity-violating weak decay of hyperons offers a means of measuring their polarization, which could help discern their production mechanisms and identify their excitation spectra, no such study has been possible for doubly strange baryons in photoproduction, due to low production cross sections. However, by making use of the reaction $\gamma p \rightarrow K^+ K^+ \Xi^-$, we have measured, for the first time, the induced polarization, P, and the transferred polarization from circularly polarized real photons, characterized by C_x and C_z, to recoiling Ξ^-s. The data were obtained using the CEBAF Large Acceptance Spectrometer (CLAS) at Jefferson Lab for photon energies from just over threshold (2.4 GeV) to 5.45 GeV. These first-time measurements are compared, and are shown to broadly agree, with model predictions in which cascade photoproduction proceeds through the decay of intermediate hyperon resonances that are produced via relativistic meson exchange, offering a new step forward in the understanding of the production and polarization of doubly-strange baryons.

Keywords: polarization, cascade, Xi, photoproduction, CLAS, hyperon, strange, hadron spectroscopy

1. Introduction

The polarization of hyperons can be measured through the angular distribution of their parity-violating weak decay products, providing insight into the mechanisms behind their production. Such measurements involving the photo- and electroproduction of Strangeness number $S = -1$ hyperons [1–12] have led to significant progress in understanding the excitation spectrum of $S = 0$ nucleons [13–25]. A similar opportunity exists in studying the polarization of $S = -2$ cascades, which could prove vital for understanding their production mechanism and in gaining an understanding of the excitation spectrum of $S = -1$ hyperons. However, because of the cascade's low production cross section and the resulting lack of available data, no previous cascade polarization measurements exist in either photo- or electroproduction.

The CLAS collaboration has reported cross-section measurements for cascade photoproduction [26, 27]. In these data, a strong back-angle peaking in the center-of-momentum cascade angular distribution ($\cos \theta_\Xi$) was observed, which along with the invariant mass distributions of the $K^+ \Xi^-$ system, suggested the significant role that intermediate hyperon resonances with masses of about 2 GeV play in cascade photoproduction. These results generated theoretical interest in understanding the production mechanism behind $S = -2$ states. In particular, Refs. [28, 29] found it is necessary to include the contributions from the decay of high-mass hyperons (up to $\Lambda(1890)$) that are predominantly produced in t-channel K/K^* exchange, as illustrated in Fig. 1, to explain the CLAS cross-section measurements [27]. Furthermore, Ref. [29] investigated the role of the addition of high-spin hyperon states around 2 GeV and found significant contributions from spin/parity $J^P = \frac{5}{2}^\pm$ and $\frac{7}{2}^\pm$ resonances. In particular, the inclusion of the $\Sigma(2030)\frac{7}{2}^+$ state improved the model's agreement with the data.

These earlier photoproduction data from CLAS did not have either beam or target polarization, and no study

on induced polarization was carried out. But as pointed out in Ref. [29], both the induced and transferred polarization of the cascade ground state are sensitive to the production mechanism, particularly, the mass, spin and parity of intermediate hyperon resonances, as well as to the mesonic exchange mechanisms.

The majority of early data for hyperon and cascade spectroscopy was generated using K^- beams on nuclear targets. However, the significance of the $Y^* \rightarrow K\Xi$ decay has never been firmly established except for the small branching ratios and branching-ratio upper limits reported for $\Lambda(2100)\frac{7}{2}^-$ and $\Sigma(2030)\frac{7}{2}^+$ [30–33] in the 1960's and 1970's. In general, the excitation spectrum for $S = -1$ hyperons also remains under-explored, particularly in the high mass (> 2 GeV) region. When compared with model predictions, cascade polarization measurements can build on the evidence for or against intermediate hyperon resonances as the dominant production mode, discriminate among the candidate exchange mechanisms, and even point to the existence of higher mass/spin hyperons.

The understanding of the ground state cascade production mechanism is not limited to its connection to the intermediate hyperon resonances. The current spectrum of experimentally established excited cascade states has remained virtually unchanged in the past thirty years [34]. At present, just six states are considered to have solid experimental evidence, and only half of these have established spin and parity. Furthermore, the number of cascade (as well as hyperon) states that appear in the most recent lattice QCD calculations [35] are nearly as numerous as predicted by early constituent quark models [36]. Understanding the production of excited cascades cannot be fully achieved without a better understanding of the ground state production, including polarization measurements. This manuscript reports the first measurements of both induced and transferred polarization of cascade baryons in photoproduction.

2. Experimental Details

A large-statistics dataset with an integrated luminosity of 68 pb^{-1} was collected with CLAS [37] using a circularly polarized, tagged photon beam [38] of energy range 1.1 to 5.4 GeV incident on a liquid hydrogen target [39]. The photon beam was produced from a longitudinally polarized primary electron beam of energy 5.7 GeV, incident on a gold radiator. The electron-beam's helicity was flipped pseudo-randomly at a rate of 30 Hz and was measured periodically by a Møller polarimeter, yielding a degree of polarization of 0.68,
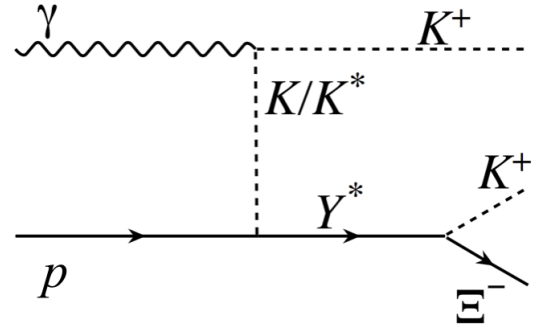

Figure 1: A possible Feynman diagram of Ξ^- photoproduction via the decay of intermediate hyperon resonances in t-channel K/K^* exchange, which is a major component in the production models of Nakayama [28, 29].

averaged over the entire run period. The degree of circular photon polarization was calculated and is known to be proportional to the electron beam polarization, and to increase as a function of the ratio of photon energy to the energy of the primary electron beam [40]. The target consisted of a 40-cm-long cylindrical cell containing liquid hydrogen. Momentum information for charged particles were obtained via tracking through three regions of multiwire drift chambers [41], with the region-two drift chambers inside a toroidal magnetic field that was generated by six superconducting coils. Scintillators [42] outside of the drift chambers were used to measure time-of-flight (TOF) information, which, when combined with the momentum information, provided charged-particle identification.

3. Analysis

Initial event selection required timing coincidences between the photon tagger and the passage of two charged particles through the CLAS detector. The photons that produced the event were selected using vertex information obtained from tracking, and the timing information from a start counter [43], which surrounded the target. The time that an event occurred at its vertex, as measured by the start counter, was required to be within ±1 ns of the photon time provided by the accelerator radio-frequency signal. Furthermore, the vertex time determined from the TOF system was required to be within ±1 ns of the photon time for all detected charged particles.

The next step in the identification of the $\gamma p \rightarrow K^+ K^+ \Xi^-$ reaction with the subsequent decay of $\Xi^- \rightarrow \Lambda \pi^-$ was selecting events with three charged mesons,
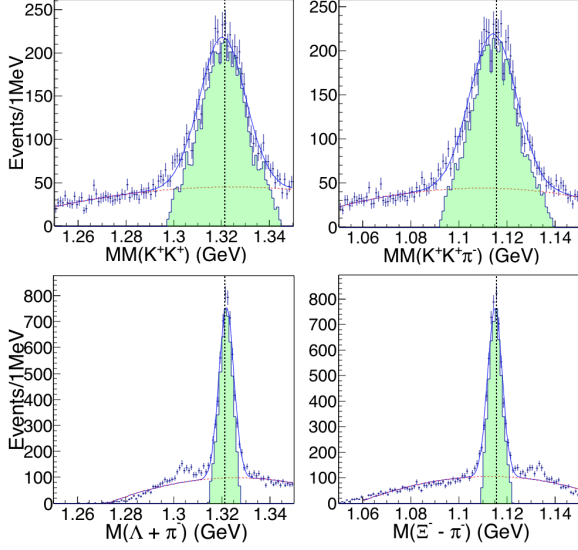
Figure 2: Mass distributions for all events passing cuts on timing, detected particle mass, and vertex location are shown by the data points with error bars. Top left: Missing mass spectrum of the K^+K^+ system; Top right: Missing mass spectrum of the $K^+K^+\pi^-$ system; Bottom left: Invariant mass spectrum of the $\Lambda\pi^-$ system; Bottom right: Invariant mass spectrum as reconstructed from the four-momentum difference of the Ξ^- and π^- system. In all plots, a Gaussian is fit to the signal over a polynomial background (dashed red line). The same distributions after applying the hypersphere cuts are shown by the filled histograms. The vertical lines represents the known Λ or Ξ^- masses. Detection of the π^- originating the Λ decay, rather than the Ξ^- decay, is evident in the left and right of the signal region, in the bottom left and bottom right plots, respectively.

K^+, K^+, and π^-, detected. Their momentum was corrected for the energy loss in the target region, as well as other detector effects such as misalignments and errors in the magnetic field map. The signals were then extracted using the following four mass distributions:

1. Missing mass in the $\gamma p \rightarrow K^+K^+(X)$ reaction, where X indicates the missing particle, labeled as $MM(K^+K^+)$.

2. Missing mass in the $\gamma p \rightarrow K^+K^+\pi^-(X)$ reaction, where X indicates the missing particle, labeled as $MM(K^+K^+\pi^-)$.

3. Invariant mass of the $(\Lambda + \pi^-)$ system, labeled as $M(\Lambda+\pi^-)$, and where the known Λ mass, 1115.683 GeV [44], was combined with the missing three-momentum of the $K^+K^+\pi^-$ system to define the Λ four-momentum vector.

4. Invariant mass reconstructed from the four-momentum difference of the Ξ^- and π^- system, labeled as $M(\Xi^- - \pi^-)$, and where the known Ξ^- mass, 1321.71 GeV [44], was combined with the
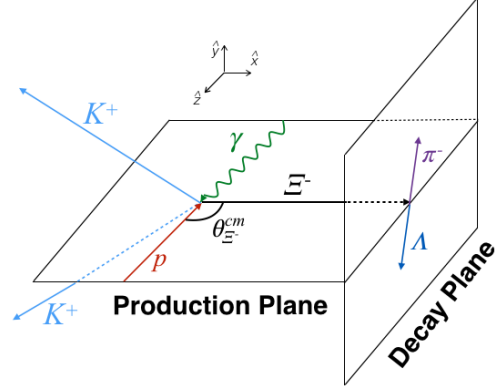

Figure 3: Plane and angle definitions for the polarization observables of C_x, C_z, and P. See the text for a full description of the coordinates.

missing three-momentum of the K^+K^+ system to define the Ξ^- four-momentum vector.

The mass distributions for events passing cuts on event timing, event vertex location, and detected particle mass are shown by the data points with error bars in Fig. 2. Clear signals for the Λ and Ξ^- are seen.

Instead of cutting on individual mass distributions, each of the above quantities was scaled by the reciprocal of their individually associated 3σ width, and treated as orthogonal displacements in a four dimensional space. A composite cut was then placed on the volume of the hypersphere that was constructed from the scaled displacements. The width σ, of each mass distribution was measured by fitting it with a Gaussian plus a polynomial to model the signal and background, as shown by the fits in Fig. 2. The hypersphere coordinates were defined as,

$$x_1 = \left[MM\left(K^+K^+\right) - \Xi^-_{mass}\right]/3\sigma_1, \qquad (1)$$
$$x_2 = \left[MM\left(K^+K^+\pi^-\right) - \Lambda_{mass}\right]/3\sigma_2,$$
$$x_3 = \left[M\left(\Lambda + \pi^-\right) - \Xi^-_{mass}\right]/3\sigma_3,$$
$$x_4 = \left[M\left(\Xi^- - \pi^-\right) - \Lambda_{mass}\right]/3\sigma_4,$$
$$r = \sqrt{x_1^2 + x_2^2 + x_3^2 + x_4^2},$$

where σ_n denotes the Gaussian width of the associated quantity as displayed in Fig. 2. A cut on the hypersphere radius r represents a simultaneous cut on all four mass quantities, where a 3σ cut corresponds to taking events within the hypervolume defined by $r < 1$. This cut, as opposed to simply rectangular cuts on the masses, allowed the best signal to background ratio, even though x_i's are not totally independent. The final data sample of 5143 events are shown in the filled histograms in Fig. 2.

The Ξ^- polarization is related to the angular distribution of the decay π^- as measured in the rest frame of the

Ξ^- by [45]

$$I(\cos\theta_\pi^{\hat{i}}) = \frac{N}{2}(1 - P_{\Xi_i}\alpha\cos\theta_\pi^{\hat{i}}),\qquad(2)$$

where $\theta_\pi^{\hat{i}}$ is the pion angle relative to the $i = x, y,$ or z axes in the Ξ^- rest frame, N is the total number of events in the $I(\cos\theta_\pi^{\hat{i}})$ distribution, P_{Ξ_i} is the i-component of the Ξ^- polarization, and α is the Ξ^- weak-decay asymmetry or analyzing power with $\alpha = -0.458\pm0.012$ [34]. The axes are defined in the Ξ^- rest-frame (Fig. 3) as

$$\hat{z} = \frac{\vec{p}_\gamma}{|\vec{p}_\gamma|},\qquad(3)$$
$$\hat{y} = \frac{\hat{z}\times\vec{p}_\Xi}{|\hat{z}\times\vec{p}_\Xi|},$$
$$\hat{x} = \hat{y}\times\hat{z},$$

where $\vec{p}_\gamma$ and $\vec{p}_\Xi$ are the photon and cascade momentum vectors, respectively, both in the center-of-momentum frame of the beam-plus-target system. The spin observables P, C_x, and C_z are connected to the recoil polarization $\vec{P}_\Xi$ through,

$$P_{\Xi_x} = P_\odot C_x,$$
$$P_{\Xi_y} = P,\qquad(4)$$
$$P_{\Xi_z} = P_\odot C_z,$$

where $P_\odot$ is the degree of photon-beam polarization.

The induced polarization, P, can be extracted from the forward-backward asymmetry, A_y, of the pion angular distribution. This method has the advantage of the cancelation of detector-acceptance effects, which follows from the fact that the polarization axis $\hat{y}$ points isotropically in the lab frame. The asymmetry is defined as,

$$A_y \equiv \frac{N_y^+ - N_y^-}{N_y^+ + N_y^-},\qquad(5)$$

where N_y^+ and N_y^- represent the number of events with $\cos\theta_\pi^y$ as positive and negative, respectively. The asymmetry is related to the induced Ξ^- polarization by

$$P = \frac{-2A_y}{\alpha}.\qquad(6)$$

The double polarization observables C_x and C_z characterize the transferred polarization of the photon to the Ξ^- and are extracted from the photon-helicity asymmetry,

$$A = \frac{N_{\text{hel}}^+ - N_{\text{hel}}^-}{N_{\text{hel}}^+ + N_{\text{hel}}^-},\qquad(7)$$

where N_{hel}^+ and N_{hel}^- are the number of events associated with positive and negative photon-beam helicity states,
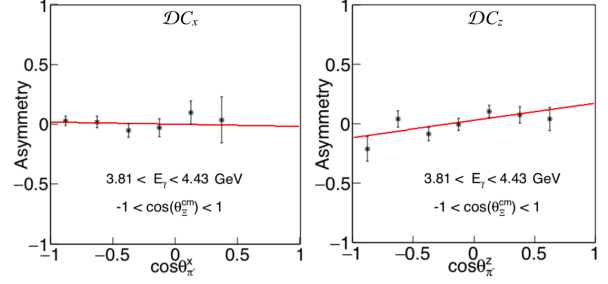

Figure 4: Above shows the beam helicity asymmetries across x and z for the Ξ^- decay, the slopes of which, along with the dilution factor, $\mathcal{D}$, are used to calculate C_x and C_z. The events displayed include all angles between Ξ^- and the z-axis but are limited to one photon energy bin.

respectively. The transferred polarization is related to the photon-helicity asymmetry by

$$\frac{-A(\cos\theta_\pi^{\hat{i}})}{|P_\odot|\alpha} = C_i\cos\theta_\pi^{\hat{i}}.\qquad(8)$$

The value and uncertainty of C_i can thus obtained from the slope of $A\cos\theta_\pi^{\hat{i}}$. Examples of the linear fits used to extract C_x and C_z are shown in Fig. 4. In the asymmetry defined in Equation 7, systematic effects such as detector acceptance mostly cancel, since they occur irrespective of the photon helicity.

It was found that overall around 15% of the events surviving the final cuts were unpolarized background events. The fraction of these events were estimated in each kinematic bin by evaluating the background subtracted yield through a Gaussian fit with a polynomial background. These events were found to have polarizations consistent with zero, thus reducing the measured polarization by the dilution factor,

$$\mathcal{D} = 1 - f_{\text{BG}},\qquad(9)$$

where f_{BG} is the fraction of background events in each sample. In order to recover the true polarization, the measured polarization observables in each bin were divided by the corresponding dilution factor, the values of which were found to be between 0.82 and 0.91.

Aside from the dilution factor, three main sources of systematic uncertainty contributed to the overall uncertainties in the measurements. For one, systematic effects due to acceptance-related factors, including the selection of the fiducial region of the detector, were estimated by comparing the final results obtained with and without these cuts, and were found to be, integrating over all kinematic bins, $\delta_{acc}P = 0.022$, $\delta_{acc}C_x = 0.01$ and $\delta_{acc}C_z = 0.052$. Additionally, uncertainty in the degree of photon-beam polarization, which in turn resulted

from the uncertainty in the primary electron beam polarization, contributed a relative scale-type uncertainty of $\delta_P C_i/C_i = 0.03$. Finally, the uncertainty in the analyzing power of the cascade, which is ± 0.012 [34], leads to a relative scale-type uncertainty of $\delta_\alpha P/P = \delta_\alpha C_i/C_i = 0.026$. For both the induced and transferred polarization measurements, the statistical uncertainty dominates the cumulative systematic uncertainty.

4. Results & Comparison With Theory

In the extraction of P, data were binned into nine regions defined by three bins of the cascade angle between the photon and target momenta in the c.m. frame with event-weighted average values of $\cos\theta_\Xi = -0.79$, -0.41, and 0.19, and three bins of photon energy with event-weighted averages of $E_\gamma = 3.47$, 4.09, and 4.88 GeV. Since the extractions of C_x and C_z require more events to achieve the same statistical uncertainty as P, these variables were binned into only three regions of $\cos\theta_\Xi$ and summed over $2.8 \leq E_\gamma \leq 5.5$ GeV, or conversely, binned into three regions of E_γ and summed over $-1 \leq \cos\theta_\Xi \leq 1$. The P results are given in Table 1 and the C_x and C_z results are given in Table 2, as well as shown in Figs. 5, 6, and 7. These results can be found in Ref. [46].

E_γ (GeV)	$\cos\theta_\Xi$	P	$\delta_{stat}P$	$\delta_{sys}P$	$\delta_{total}P$	$\delta_{scl}P/P$
3.47	−1 to 1	−0.011	0.12	0.022	0.12	0.026
4.09	−1 to 1	−0.089	0.12	0.022	0.12	0.026
4.88	−1 to 1	0.006	0.13	0.022	0.13	0.026
2.8 to 5.5	−0.79	−0.045	0.12	0.022	0.12	0.026
2.8 to 5.5	−0.41	0.15	0.12	0.022	0.12	0.026
2.8 to 5.5	0.19	−0.19	0.12	0.022	0.12	0.026
3.47	−0.80	−0.088	0.21	0.022	0.21	0.026
4.10	−0.79	−0.14	0.20	0.022	0.20	0.026
4.86	−0.77	0.036	0.22	0.022	0.22	0.026
3.45	−0.44	0.15	0.20	0.022	0.20	0.026
4.09	−0.40	0.16	0.22	0.022	0.22	0.026
4.88	−0.36	0.10	0.22	0.022	0.22	0.026
3.50	0.12	−0.10	0.20	0.022	0.20	0.026
4.10	0.19	−0.27	0.21	0.022	0.21	0.026
4.90	0.26	−0.12	0.21	0.022	0.22	0.026

Table 1: Summary of P measurements and uncertainties. The values of E_γ and $\cos\theta_\Xi$ given are the means of their distributions within each bin.

For comparison, the polarization predictions of the three phenomenological model variants put forth by Refs. [28, 29] to help explain the differential cross sections reported by Ref. [27], overlay our results in Figs. 5, 6, and 7. All three model variants share the same framework, in which cascade photoproduction

E_γ (GeV)	$\cos\theta_\Xi$	C_x	$\delta_{stat}C$	$\delta_{sys}C$	$\delta_{total}C$	$\delta_{scl}C/C$
3.47	−1 to 1	0.21	0.39	0.01	0.39	0.039
4.09	−1 to 1	−0.083	0.34	0.01	0.34	0.039
4.88	−1 to 1	−0.021	0.32	0.01	0.32	0.039
2.8 to 5.5	−0.79	−0.21	0.33	0.01	0.33	0.039
2.8 to 5.5	−0.41	0.37	0.35	0.01	0.40	0.039
2.8 to 5.5	0.19	0.012	0.40	0.01	0.40	0.039

E_γ (GeV)	$\cos\theta_\Xi$	C_z	$\delta_{stat}C$	$\delta_{sys}C$	$\delta_{total}C$	$\delta_{scl}C/C$
3.47	−1 to 1	0.52	0.35	0.052	0.35	0.039
4.09	−1 to 1	0.67	0.29	0.052	0.29	0.039
4.88	−1 to 1	0.001	0.26	0.052	0.26	0.039
2.8 to 5.5	−0.79	0.52	0.32	0.052	0.33	0.039
2.8 to 5.5	−0.41	0.49	0.28	0.052	0.29	0.039
2.8 to 5.5	0.19	0.13	0.30	0.052	0.30	0.039

Table 2: Summary of C_x and C_z measurements and uncertainties.

proceeds through the decay of intermediate hyperon resonances that are produced via relativistic meson exchange. The predictions are based on pseudoscalar (solid red) and pseudovector (dashed blue) relativistic meson-exchange. Contributions from the $\Sigma(2030)$, which has spin-7/2, were introduced in Ref. [29] (dotted green).

The predicted values of P and C_x follow fairly flat curves, that when determined over the entire angular and/or energy range, integrate to nearly zero. Conversely, the predicted values of C_z are positive and sizable over the kinematic range and thus do not integrate to zero on any interval.

As shown in Figs. 5, 6, and 7, our measurements are generally well described by the pseudoscalar (solid red) and the 2011 pseudovector (dotted green) models but not the 2006 pseudovector model (dashed blue). We have performed a statistical comparison of the three model variants to 15 independent data points, 9 of which come from the induced polarization, P, in the unintegrated binning scheme in Table 1, while the other 6 data points come from the transferred polarization, C_x and C_z, summed over E_γ. The agreement between the data and the pseudoscalar variant is good, with a $\chi^2 = 13.0$. The 2006 variant of the pseudovector model has $\chi^2 = 33.0$ and is therefore excluded by the data with $\sim 99\%$ confidence. The 2011 variant of the pseudoscalar model (dotted green) has $\chi^2 = 17.4$. Similar results are found when comparing the model to the $\cos\theta_\Xi$ integrated transferred polarization results. However it is import to point out these models were tested against the cross sections measurements up to around 4 GeV. Above that, it is possible that other mechanisms not accounted for such as the Regge trajectories and other higher-mass hyperons might need to be included.

Finally, it is worth pointing out that the photoproduced Λ was observed [8] to exhibit nearly 100% po-
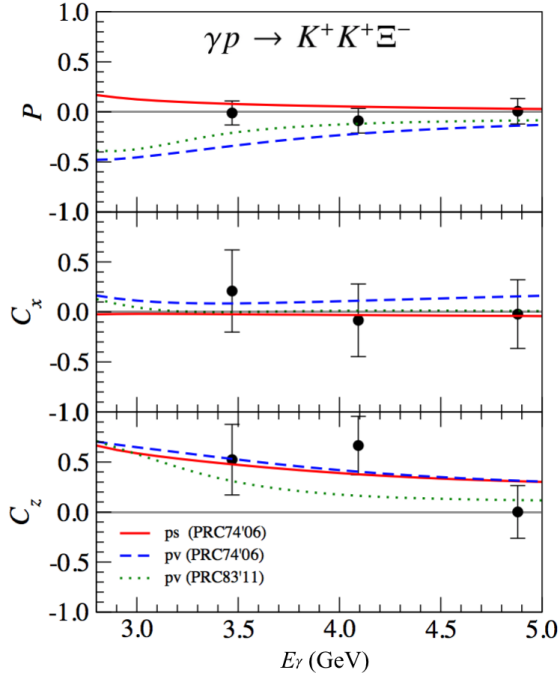
Figure 5: P (top), C_x (middle) and C_z (bottom) as a function of E_γ and summed over $\cos\theta_\Xi$. The error bars represent the total uncertainty. The legend specifies pseudoscalar (ps) or pseudovector (pv) coupling, as well as the journal of publication for the associated model.

Figure 6: P (top), C_x (middle) and C_z (bottom) as a function of $\cos\theta_\Xi$ and summed over E_γ. Error bars and curves are the same as in Fig. 5.

larization by evaluation of $R = \sqrt{C_x^2 + C_z^2 + P^2}$. This quantity for the Ξ^-, integrating our results over all bins, is 0.30 ± 0.14, which is non-zero but significantly smaller than the Λ counterpart.

5. Conclusion

To summarize, we have made the first polarization measurements for the Ξ^- in photoproduction by measuring the induced polarization, P, as well as transferred polarization, C_x and C_z, using a circularly polarized photon beam. We have found that the total integrated Ξ^- polarization departs from zero by 2σ, but is significantly smaller than in the analogous case for Λ photoproduction. The results have been compared, and show general agreement with the predictions of a phenomenological model of cascade photoproduction involving intermediate hyperon resonances that are produced, predominantly in the t-channel, via relativistic pseudoscalar meson exchange. The results strongly disfavored a model variant that includes significant contributions from the $\Sigma(2030)\frac{7}{2}^+$. While precisely distinguishing between current and future model variants to
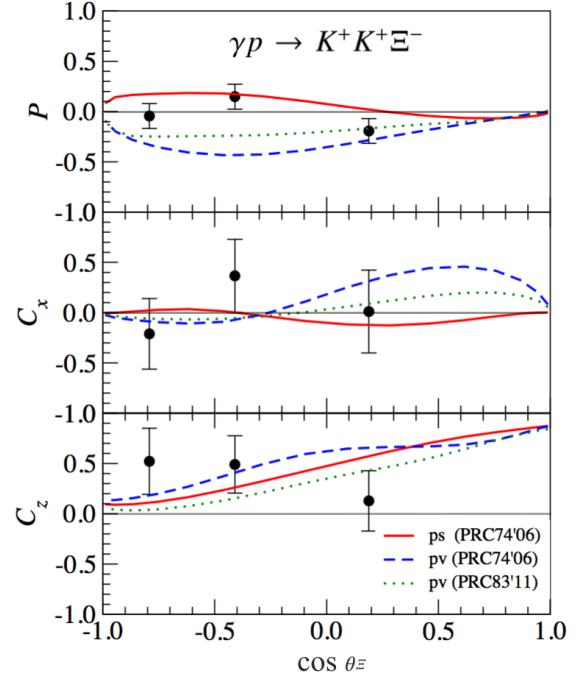
determine the role of high-spin excited hyperons and the contributions from scalar versus vector exchange mechanisms will be left to future experiments at CLAS12 and GlueX [47], we have made the first step toward a detailed understanding of Ξ^- photoproduction.
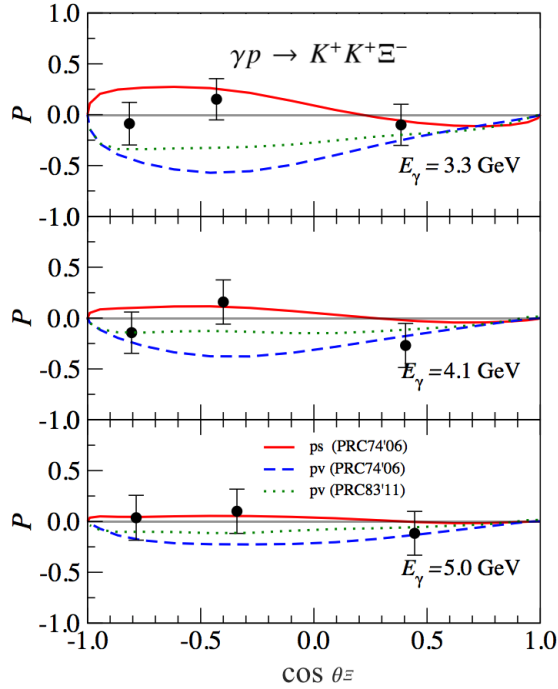
6. Acknowledgments

Figure 7: P as a function of $\cos\theta_\Xi$ for three E_γ bins as indicated. Error bars and curves are the same as in Fig. 5.

ergy, Office of Nuclear Physics, under contracts No. de-sc0013620.

7. Bibliography

[1] C. A. Paterson, et al., Photoproduction of Λ and Σ^0 hyperons using linearly polarized photons, Phys. Rev. C 93 (2016) 065201.

[2] M. Q. Tran, et al., Measurement of $\gamma p \to K^+\Lambda$ and $\gamma p \to K^+\Sigma^0$ at photon energies up to 2 GeV, Phys. Lett. B445 (1998) 20–26.

[3] D. S. Carman, et al., First measurement of transferred polarization in the exclusive polarized $ep \to e'K^+\Lambda$ reaction, Phys. Rev. Lett. 90 (2003) 131804.

[4] K. H. Glander, et al., Measurement of $\gamma p \to K^+\Lambda$ and $\gamma p \to K^+\Sigma^0$ at photon energies up to 2.6 GeV, Eur. Phys. J. A19 (2004) 251–273.

[5] R. G. T. Zegers, et al., Beam polarization asymmetries for the $p(\gamma, K^+)\Lambda$ and $p(\gamma, K^+)\Sigma^0$ reactions at $E(\gamma)$ = 1.5 GeV - 2.4 GeV, Phys. Rev. Lett. 91 (2003) 092001.

[6] J. W. C. McNabb, et al., Hyperon photoproduction in the nucleon resonance region, Phys. Rev. C69 (2004) 042201.

[7] M. Sumihama, et al., The Polarized $\gamma p \to K^+\Lambda$ and polarized $\gamma p \to K^+\Sigma^0$ reactions at forward angles with photon energies from 1.5-GeV to 2.4-GeV, Phys. Rev. C73 (2006) 035214.

[8] R. Bradford, et al., First measurement of beam-recoil observables C_x and C_z in hyperon photoproduction, Phys. Rev. C75 (2007) 035205.

[9] M. McCracken, et al., Differential cross section and recoil polarization measurements for the $\gamma p \to K^+\Lambda$ reaction using CLAS at Jefferson Lab, Phys. Rev. C81 (2010) 025201.

[10] B. Dey, et al., Differential cross sections and recoil polarizations for the reaction $\gamma p \to K^+\Sigma^0$, Phys. Rev. C82 (2010) 025202.

[11] D. S. Carman, et al., Beam-Recoil Polarization Transfer in the Nucleon Resonance Region in the Exclusive $\vec{e}p \to e'K^+\vec{\Lambda}$ and $\vec{e}p \to e'K^+\vec{\Sigma}^0$ Reactions at CLAS, Phys. Rev. C79 (2009) 065205.

[12] M. Gabrielyan, et al., Induced polarization of $\Lambda(1116)$ in kaon electroproduction, Phys. Rev. C90 (3) (2014) 035202.

[13] A. V. Anisovich, V. Kleber, E. Klempt, V. A. Nikonov, A. V. Sarantsev, U. Thoma, Baryon resonances and polarization transfer in hyperon photoproduction, Eur. Phys. J. A34 (2007) 243–254.

[14] V. A. Nikonov, A. V. Anisovich, E. Klempt, A. V. Sarantsev, U. Thoma, Further evidence for N(1900) P(13) from photoproduction of hyperons, Phys. Lett. B662 (2008) 245–251.

[15] A. V. Anisovich, E. Klempt, V. A. Nikonov, A. V. Sarantsev, U. Thoma, P-wave excited baryons from pion- and photo-induced hyperon production, Eur. Phys. J. A47 (2011) 27.

[16] A. V. Anisovich, E. Klempt, V. A. Nikonov, A. V. Sarantsev, U. Thoma, Nucleon resonances in the fourth resonance region, Eur. Phys. J. A47 (2011) 153.

[17] A. V. Anisovich, E. Klempt, V. A. Nikonov, A. V. Sarantsev, U. Thoma, Evidence for a spin-quartet of nucleon resonances at 2 GeV, Phys. Lett. B711 (2012) 167–172.

[18] A. de la Puente, O. V. Maxwell, B. A. Raue, New fits to the reaction $\gamma p \to K^+\Lambda$, Phys. Rev. C80 (2009) 065205.

[19] O. V. Maxwell, Beam polarization asymmetry and the electromagnetic production of kaons from protons, Phys. Rev. C86 (2012) 064612.

[20] O. V. Maxwell, Model for the electroproduction of kaons and Λ's from the deuteron, Phys. Rev. C89 (2) (2014) 024001.

[21] O. V. Maxwell, New fit to the reaction $\gamma p \to K^+\Sigma^0$, Phys. Rev. C92 (4) (2015) 044614.

[22] O. V. Maxwell, Electromagnetic production of K mesons from the proton: A new fit to recent data, Phys. Rev. C93 (1) (2016) 014605.

[23] G. Penner, U. Mosel, Vector meson production and nucleon resonance analysis in a coupled-channel approach for energies $m_N < \sqrt{s} < 2$ GeV II: photon-induced results, Phys. Rev. C66 (2002) 055212.

[24] M. Döring, et al., The reaction $\pi^+p \to K^+\Sigma^+$ in a unitary coupled-channels model, Nucl. Phys. A851 (2011) 58.

[25] H. Kamano, S. Nakamura, T.-S. Lee, T. Sato, Extraction of P_{11} resonances from πN data, Phys. Rev. C81 (2010) 065207.

[26] J. W. Price, et al., Exclusive photoproduction of the cascade Xi hyperons, Phys. Rev. C71 (2005) 058201.

[27] L. Guo, et al., Cascade production in the reactions $\gamma p \to K^+K^+(X)$ and $\gamma p \to K^+K^+\pi^-(X)$, Phys. Rev. C76 (2007) 025208.

[28] K. Nakayama, Y. Oh, H. Haberzettl, Photoproduction of Ξ off nucleons, Phys. Rev. C74 (2006) 035205.

[29] J. K. S. Man, Y. Oh, K. Nakayama, Role of high-spin hyperon resonances in the reaction of $\gamma p \to K^+K^+\Xi^-$, Phys. Rev. C83 (2011) 055201.

[30] P. J. Litchfield, et al., K^-p elastic and charge-exchange scattering in the c.m. energy range $1915 - 2168$ MeV, Nucl. Phys. B30 (1971) 125.

[31] R. A. Muller, A Study Of The Reaction $K^-N \to \Xi K$ From threshold To 2.7-GeV/c, Ph.D. thesis, LBL, Berkeley (1969).

[32] R. D. Tripp, et al., Baryon Resonances In SU(3), Nucl. Phys. B3 (1967) 10.

[33] G. Burgun, et al., Resonance formation in the reactions $K^-p \to K^+\Xi^-$ and $K^-p \to K^0\Xi^0$ in the mass region from 1915 to 2168 MeV, Nucl. Phys. B8 (1968) 447.

[34] C. Patrignani, et al., Review of Particle Physics, Chin. Phys. C40 (10) (2016) 100001.

[35] R. Edwards, et al., The Flavor Structure of the Excited Baryon

Spectra from Lattice QCD, Phys. Rev. D87 (2013) 054506.

[36] S. Capstick, N. Isgur, Baryons in a relativized quark model with chromodynamics, Phys. Rev. D34 (1986) 2809.

[37] B. A. Mecking, et al., The CEBAF Large Acceptance Spectrometer (CLAS), Nucl. Instrum. Meth. A503 (2003) 513–553.

[38] D. I. Sober, et al., The bremsstrahlung tagged photon beam in Hall B at JLab, Nucl. Instrum. Meth. A440 (2000) 263–284.

[39] G12 experimental group, CLAS-NOTE 2017 − 002, (2017), `https://misportal.jlab.org/ul/Physics/Hall-B/clas/viewFile.cfm/2017-002.pdf?documentId=756`.

[40] H. Olsen, L. C. Maximon, Photon and Electron Polarization in High-Energy Bremsstrahlung and Pair Production with Screening, Phys. Rev. 114 (1959) 887–904.

[41] M. D. Mestayer, et al., The CLAS drift chamber system, Nucl. Instrum. Meth. A449 (2000) 81–111.

[42] E. S. Smith, et al., The time-of-flight system for CLAS, Nucl. Instrum. Meth. A432 (1999) 265–298.

[43] Y. G. Sharabian, et al., A new highly segmented start counter for the CLAS detector, Nucl. Instrum. Meth. A556 (2006) 246–258.

[44] C. Patrignani, et al., Review of Particle Physics, Chin. Phys. C40 (10) (2016) 100001.

[45] M. Huang, et al., New measurement of $\Xi^- \to \Lambda\pi^-$ decay parameters, Phys. Rev. Lett. 93 (2004) 011802.

[46] Data reported here may be accessed in the CLAS Physics Database at:. `http://clas.sinp.msu.ru/cgi-bin/jlab/db.cgi`.

[47] M. Dugger, et al., A study of decays to strange final states with GlueX in Hall D using components of the BaBar DIRC ,`arXiv: 1408.0215`.